The Effect of Hydrogen Absorption on the Structural, Electronic and Magnetic Properties of the C15 Friauf-Laves Phase Compounds CeFe$_2$, CeRu$_2$ and LaRu$_2$: an X-Ray Absorption Spectroscopy (XAS) Study

Jesús Chaboy and Joaquin García
Instituto de Ciencia de Materiales de Aragón ICMA, CSIC-Universidad de Zaragoza,
50009 Zaragoza, Spain

Augusto Marcelli
I. N. F. N., Laboratori Nazionali di Frascati, Casella Postale 13, 00044 Frascati, Italy

Abstract

We present an x-ray absorption spectroscopy (XAS) investigation of the structural changes occurred upon hydriding in the Friauf-Laves phase compounds CeFe$_2$, CeRu$_2$ and LaRu$_2$ compounds. The analysis of the extended x-ray absorption spectroscopy (EXAFS) spectra at the L-edges of the rare-earth and at the Fe K-edge indicates that the hydrogenation process leads to the suppression of the long-range crystalline order in all the hydride derivatives investigated, as well as the different influence of H$_2$ in both the rare earth and transition metal sublattices. The correlation between the structural and magnetic changes induced by the hydrogen in the host matrix is discussed in terms of the modification of the electronic properties, i.e., intermediate-valence state of Ce, and of the hybridization between the transition metal and the rare-earth.

Submitted to Physical Review B

I. INTRODUCTION

The investigation of the magnetic properties of intermetallic rare earth (R) and 3d transition-metal (M) compounds focuses substantial amount of research because these compounds are of particular interest for technological application. Although the relatively low magnetocrystalline anisotropy in R-Fe compounds and the exceptionally low Curie temperature make them less attractive for application as permanent magnet materials, considerable improvements with respect to the ordering temperature can be achieved upon hydrogen absorption.

In the last years, a large body of information has been accumulated regarding hydrogen absorption by intermetallic materials. Initial interest was devoted to the technological application of these materials: energy conversion in solar heating and cooling, hydrogen storage, hydrogen compressors, cold accumulators and hydrogen based batteries [1,2]. However, hydrogen absorption leads to strong changes of the macroscopic structural and magnetic properties of these materials, so that nowadays the interest has turned to understand not only the mechanism responsible for hydrogen absorption by intermetallic compounds but also to ascertain its effect on the magnetic, structural and electronic properties.

Cerium the least expensive of all the rare earth elements, when present in a trivalent state can give rise to rare earth anisotropies much larger than those of other rare earth elements. Unfortunately, cerium has a preference to be non-magnetic when combined with 3d metals, which hampers the application of most cerium-based intermetallic compounds as permanent magnet materials. In the last years, however, several reports addressed the induction of a change of the Ce electronic state driven by interstitial doping, thus opening a new route towards the development of Ce-based permanent-magnet materials. This result bears to an increasing interest into studying how the electronic structure of Ce ions in Ce-Fe rich alloys is modified upon hydrogen absorption. This topic is nowadays a matter of controversy. Indeed, whereas several authors claim for the existence of a Ce^{4+} to Ce^{3+} transition taking place upon hydrogen absorption, according to the analysis of the lattice parameters expansion

[3–6], both recent energy-band calculations and XAS investigations point on the role played by the hybridization among 4f and 5d and/or 3d electrons into driving the modification of the magnetic properties of these systems [7–11].

The large class of RM_2-type Laves phases offer a good chance to study the correlation between the structural and electronic modifications associated to the H_2 uptake absorption and to obtain a deeper insight about the possible mechanism, the modification of the Ce valence or the R-M hybridization, that drives the changes in the magnetic behavior of these materials. This family has been object of a great deal of research by exhibiting the most desirable storage characteristics such as hydrogen capacities and rapid hydriding-dehydriding kinetics together with a quite simple crystal structure [12–16]. To this family belongs $CeFe_2$ and $CeRu_2$, two of the Ce-based materials showing the most dramatic changes in their magnetic properties upon H_2 uptake.

$CeFe_2$ is a simple ferromagnet with a Curie temperature, T_c, of about 230 K. Its magnetization behavior and the magnetic hyperfine field follow approximately the molecular-field theory with a J=1/2 Brillouin function [13–17]. The low value of the magnetic hyperfine field has been associated to both the reduced magnetic moment of the iron ions, 1.2 μ_B, as compared to 1.7 μ_B in other RFe_2 compounds, and to the low T_c, that ranges between 500 and 700 K in other RFe_2 compounds. Due to the reduced lattice parameter of $CeFe_2$, these anomalies were early ascribed to the transfer of the Ce $4f$ electron to the conduction band, resulting in the increase of the Fe $3d$-band occupancy [14,16]. However, the discovery that the substitution of Fe by a small amount of impurity destabilizes the ferromagnetism in $CeFe_2$, yielding to a spin-canting or reentrant spin-glass-like behavior for small Al substitutions [18–20], and to the total loss of ferromagnetism for 4% to 5% Al substitution [21,22], has stimulated new studies on the instability of ferromagnetism in this compound. Also $Ce(Fe_{1-x}M_x)_2$ pseudobinaries with M = (Co, Ru, Si, Os, Ir) exhibit similar magnetic instabilities [23–28], whereas no instability is associated to the M = (Ni, Cu, Rh, Mn) substitution [23,27]. Moreover, substitution of Y and U onto the Ce sites in these anomalous pseudobinaries results in a return to normal magnetic behavior [22,23,29]. All these results

question the naive picture of non-magnetic Ce in $CeFe_2$, pointing out the role of the hybridization between the $4f$ and $3d$-band electrons into determine the magnetic behavior of $CeFe_2$ and its related pseudobinaries compounds [7,30,31]. The peculiar behavior of $CeFe_2$ within the RFe_2 series is also evidenced by the marked change of its magnetic properties upon hydrogen uptake: the saturation magnetization is about 70 % higher than in the unhydrogenated compound and T_c increases up to 358 K. On the contrary, the decrease of T_c and a slight increase of the Fe magnetic moment (25% for YFe_2H_4) is observed for rest of the RFe_2 series [32,33]. The outstanding behavior of $CeFe_2$ upon hydrogen uptake has been interpreted in terms of the change in the valence state of Ce upon H_2 uptake [34,35].

$CeRu_2$ and $LaRu_2$ are largely known as notable exceptions to the magnetic behavior of most superconducting materials. In fact, $CeRu_2$ was the first discovered superconducting system in which the magnetic ions could be introduced substitutionally without adversely affecting the superconductor state [36]. Moreover, it was found that small concentrations of rare earth impurities in $CeRu_2$ enhance its superconductivity properties and that rather large concentrations can be accommodated without destroying the superconducting state [37–39]. On the contrary, substitutions on the Ru site sharply depress T_S [40]. Commonly, it has been assumed that cerium in this material is tetravalent because several studies have shown that the introduction of a localized 4f electron into various superconducting matrices drives the host T_S to zero [41]. Consequently, the superconductivity was originally assigned to the Ru-4d bands in both $CeRu_2$ and $LaRu_2$ compounds [42–44]. More recently, theoretical energy band calculations open again the debate about the origin of the electrons where superconductivity lies. Using the self-consistent APW method Yanase has shown the existence of a 4f band of appreciable width in $CeRu_2$, identifying the superconducting electrons as the 4f electrons on the Ce sites [45,46]. This interpretation can be also extended to the case of $LaRu_2$ taking into account recent resistivity results claiming for the existence of 4f electrons in $LaRu_2$ [47]. In this framework, the study of the hydrogen effect to the superconducting properties of $CeRu_2$ and $LaRu_2$ becomes a fundamental subject of research. Indeed, while the reported sudden suppression of the superconducting state in the $CeRu_2$

hydrides [48,49] has been interpreted in terms of a perfect change of the cerium valence induced by the H_2 uptake [48–51], no interpretation has been driven yet about the loss of the superconductivity state in the $LaRu_2H_x$ compounds.

In this work, we present an extensive x-ray absorption spectroscopy (XAS) study performed at the rare earth L-edges and at the Fe K-edge in the case of $CeFe_2$, $CeRu_2$ and $LaRu_2$ systems and their hydrides derivatives. This investigation has been devoted to correlate the modification of the local environment around each atomic species induced by hydrogen, as determined by extended x-ray absorption fine structure (EXAFS) analyses, with the change of the magnetic properties. The valence state of cerium has been investigated by x-ray absorption near edge structure (XANES) at the Ce L_3-edge, while measurements of the rare-earth L_1-edge and Fe K-edge XANES spectra have been performed to determine the modification of the local and partial density of states around the Fermi energy induced by the interstitial doping. These experiments clarify the interplay between the structural and magnetic changes, that are associated to both, the modification of the hybridization between the transition-metal (Ru-4d,Fe-3d) and rare-earth (5d) bands, and to the localization of $4f$ magnetic moment at the Ce sites upon hydriding.

II. EXPERIMENTAL SETUP

XAS experiments have been performed at the Fe K-edge and at the L-edges of La and Ce in the compounds $CeFe_2H_x$ with x= (0, 2.8, 3.75), $CeRu_2H_x$ with x= (0, 2.9, 4, 4.8) and $LaRu_2H_x$ (0, 2.8, 4.8).The preparation procedure of these materials and their characterization is described elsewhere [48–50].

Several samples were measured in different experimental runs at the synchrotron radiation facility of the Laboratori Nazionali di Frascati. The ADONE storage ring was operated at 1.5 GeV during dedicated beam time with an averaged current of approximately 40 mA. The x-ray radiation was monochromatized using a Si(111) channel-cut crystal. The absorption experiments were carried out at different fixed temperatures, from room temperature

down to 10 K, in the transmission mode. Both x-rays incident on the sample and transmitted through it were monitored with two independent ionization chambers using flowing gas (N_2, Ar) mixtures optimized for each different energy range. Samples were held in vacuum and formed by homogeneous thin layers. Thickness and homogeneity of the samples were optimized to obtain the best signal to noise ratio using two layers of powdered material giving a total absorption jump, $\Delta\mu x$, ranging between 0.4 and 1 as a function of the absorption edge selected. During each experimental run, both fresh and old samples were measured to establish the stability of hydrogen content. Deuterated samples used in previous investigations were also measured. No appreciable difference, other than the signal-to-noise ratio, was never observed.

The absorption spectra were analyzed according to standard procedures [52,53]. The background contribution from lower energy absorption edges, $\mu_B(E)$, was approximated according to the Victoreen rule and subtracted from the experimental spectrum $\mu(E)$. The average absorption above the edge was fitted with a smooth spline formed by three cubic polynomials to simulate the atomic-like term $\mu_0(E)$. The EXAFS signal $\chi(k)$ was then determined as $\chi(k) = (\mu - \mu_B - \mu_0)/\mu_0$, where the photoelectron wave vector k is defined by $k = \sqrt{(2m/\hbar^2)(E - E_0)}$. XANES spectra were normalized to the absorption coefficient at high energy to eliminate thickness dependence. In both cases, the energy origin E_0, corresponding to the continuum threshold was defined to be at the inflection point of the absorption edge.

III. EXAFS STRUCTURAL STUDY

$CeFe_2$, $CeRu_2$ and $LaRu_2$ compounds crystallize as the cubic (C15) Friauf-Laves RM_2 phases in which all interstices are formed by tetrahedra of variable regularity, see Fig. 1. Upon hydrogen absorption, hydrogen fills the available tetrahedral sites that are usually referred according to the atoms that occupy the apices of the tetrahedra: $B4$, $AB3$ and $A2B2$, the number of these sites per formula unit RM_2 being 1, 4 and 12 respectively [54,55]. The

behavior of the Laves phases upon hydrogen uptake has stimulated a great deal of interest due to the possibility to obtain either a crystalline hydride phase or the induction of an amorphization process. Actually, there is a strong controversy about the nature of the hydride phases in both $CeFe_2$ and $CeRu_2$ compounds, i.e., crystalline versus amorphous state. In this sense, several works have reported that the hydrogen absorption leads to the loss of the long-range crystalline order in the case of the $CeFe_2$ hydrides [32,33,56–58] as it also occurs in the case of the RNi_2 and RCo_2 alloys [59–61]. Preliminary EXAFS studies performed on the $CeFe_2$ and $CeRu_2$ hydrides reported that hydriding produces amorphization of the cerium sublattice, whereas the iron sublattice is less affected [62]. However, these results were posteriorly interpreted excluding the formation of a real amorphous state [63], in opposition to recent x-ray diffraction (XRD) studies [64].

Similar controversy holds for the $CeRu_2$ hydrides. The first crystallographic characterization of the hydride phases of $CeRu_2$ and $LaRu_2$ performed by Tessema and coworkers [48] reported that the cubic C15 structure was preserved upon hydrogen uptake, showing a relative increase of the lattice parameter of the 12% and 9% for $CeRu_2H_x$ and $LaRu_2H_x$ compounds, respectively. In addition, neutron diffraction studies led to the determination of the atomic positions occupied by the hydrogen (deuterium) atoms [49,50], in disagreement with both EXAFS [57,62] and XRD investigations [65,66] that show the amorphization of the hydride derivatives. To clarify the controversy about the modification of the host matrix induced by hydrogen absorption in both transition metal and rare-earth sublattice separately, we have carried out a systematic EXAFS analysis in these materials.

A. Fe K-edge EXAFS

The EXAFS oscillations, $\chi(k)$, at the Fe K-edge and their Fourier transforms (FT) are reported in Fig. 2 for $CeFe_2$ and its hydride derivatives $CeFe_2H_x$ with an hydrogen content of x = 2.8 and 3.75. The EXAFS signals, multiplied by k^2, were Fourier transformed using a Hanning window [67] (Δk=0.2 Å^{-1}) over the k range $2.5 \leq k \leq 10$ Å^{-1} [68].

The comparison of the Fe EXAFS signals prior and after the hydrogen uptake shows a strong smoothing of the EXAFS signal for the hydride derivatives, whereas the differences between the EXAFS for the two hydrogen concentrations are negligible. The EXAFS structures almost dissappear for the hydrides and the modulation of their EXAFS signals fits well with a single-frequency, indicating the reduction of the single and multiple-scattering paths contributing to the absorption spectra. This result can be certainly associated to the lack of long-range crystalline order, i.e., the presence of a "real" amorphous phase. The amorphization induced in the host matrix upon H_2 absorption can be also inferred from the analysis of the FT. Indeed, whereas for $CeFe_2$ the FT exhibits contributions up to 6 Å, in the case of the hydrides the contributions from atoms beyond the first coordination shell are missing. In addition, the main peak in the FT is shifted to lower R and its intensity is strongly reduced. Both results are a strong indication of the reduction of the coordination number around the absorbing Fe and of its nearest-neighbor interatomic distance.

These results are in qualitative agreement to those reported in previous EXAFS investigations [62]. However, because the existence of an amorphous phase has been excluded on the basis of high-local-disorder considerations [63], and in order to gain a deeper insight on the nature of the hydride phases, we have measured the absorption spectra as a function of temperature, as shown in Fig. 3 for the case of $CeFe_2$. The lowering of temperature makes evident the existence of contributions coming from neighbors located at distances of up to 9 Å from the absorber, and at the same time, the height of the main FT peak for the lowest temperature (15 K) is twice that of the room temperature FT. On the contrary, in the case of the hydrides no additional structures are present in the FT and the magnitude of the FT increases very slightly, in agreement with that expected under the amorphization of the system upon H_2 uptake.

In order to determine the local environment of the Fe atoms in the amorphous hydride derivatives, we performed a theoretical simulation of the EXAFS spectra at the Fe K-edge. The computations were carried out using the code EXCURVE [69]. Atomic phase-shifts and back-scattering amplitudes were calculated in the Z+1 approximation, i.e., we substitute

the atomic orbitals of Fe for those of Co imposing a 1s core-hole. Throughout the analysis, because the phase-shifts are more accurate at high k, k-cubed weighting was applied to both compensate for the diminishing amplitude at high k and to achieve a better determination of the energy shift needed to match the theoretical simulation [70].

Theoretical phase-shifts and backscattering amplitudes were tested taking $CeFe_2$ as the reference system. The knowledge of the crystal structure of the reference allows to fix both the energy-shift and S_0^2, the empirical correction for photo-electron shake-up and shake-off, that we have used in the analysis of the hydrides. In this way, the only variable parameters in the refinement process are the interatomic distances, the coordination numbers and the Debye-Waller factors.

Using the best-fit procedure in the k range $3 \leq k \leq 9.5$ Å^{-1}, the filtered spectrum of $CeFe_2$ and $CeFe_2H_{3.75}$ was compared to the theoretical simulation. The quality of the theoretical simulations can be assessed by visual comparison of the experimental and simulated EXAFS spectra and their Fourier transforms, as shown in Fig. 4, and by calculation of the fitting index [71] defined as

$$FI = \frac{1}{100npt} \sum_{i=1}^{npt} (Res_i k^{wt})^2 \qquad (1)$$

where $Res_i = \chi_i$ (calculated) - χ_i (experimental), npt is the number of data points and wt is the integral weight used to offset the decay of $\chi(k)$ as the energy increases. The values of the best-fit parameters are reported in Table I and compared to XRD data. In the case of the hydride derivative, the coordination around Fe is strongly reduced to 3 Fe neighbors and the interatomic Fe-Fe distance is shorter that in the parent $CeFe_2$ compound. Both results are consistent with an amorphization of the system upon hydrogen uptake. In fact, if the crystalline phase is retained, not only the coordination should be unchanged but also an increase of the interatomic Fe-Fe distance should be expected, due to the lattice expansion induced by hydrogen. On the contrary, our data show the breakdown of the long-range crystalline order and how the Ce atoms in the first coordination sphere around central iron in $CeFe_2$ are not present in hydrides. This result is related to the disappearance in the case

of the hydrides of the shoulder-like feature in the FT of $CeFe_2$, and directly derived from the quantitative analysis summarized in Table I.

Finally, to obtain a further test of these results, we have performed also a best-fit procedure using the experimental Fe-Fe and Fe-Ce phase-shifts and backscattering amplitudes obtained from the filtering of the K-Fe EXAFS signal of $CeFe_2$ in the ranges 1.2 to 2.5 Å and 2.5 to 3.8 Å, respectively. The results, summarized in Table I, are in agreement with those obtained by using the theoretical phase-shifts. In addition, we have extended the analysis also to the second detectable peak in the Fourier transform of the hydrides (see Fig. 2) obtaining a second coordination shell formed by Ce atoms located at 3.25 Å from the absorbing Fe.

B. Ce and La L_3-edge EXAFS

The previous analysis has clearly shown the amorphization process taking place in $CeFe_2$ upon hydrogen absorption, providing a first insight on the local structure around the transition metal in the hydride phases. In this section we present a parallel analysis performed at the Ce and La sites in order to determine the influence of hydrogen on the rare-earth sublattice and the modification of the local structure upon the H_2 uptake.

Fig. 5 shows the EXAFS spectra recorded at the L_3-edge of the rare earth in $CeFe_2$, $CeRu_2$, $LaRu_2$ and their hydrides derivatives at different hydrogen concentration. The EXAFS signals were Fourier transformed using a Hanning window ($\Delta k=0.2$ Å^{-1}) over the k range $3 \leq k \leq 10.5$ Å^{-1}. The huge decrease of the fine structure of all the hydrides derivatives is made evident, proceeding independently of the hydrogen concentration. The same result is found from the analysis of the rare-earth L_1-edge, as shown in Fig. 5, whereas in the case on $SmRu_2$ the hydride is found to retain the crystal structure. As in the case of the Fe K-edge, the smearing out of the scattering resonances confirms the amorphization of the systems upon H_2 uptake. Moreover, the reduction of the EXAFS signals after the hydrogen absorption has revealed the presence of a strong feature at about 6 Å^{-1} that has

been demonstrated to be associated to the existence of a $2p4d \rightarrow (5d)^2$ transition [57,72–76].

In order to characterize the remaining local order around the rare earth we have performed the EXAFS data analysis, as described in the previous section, by using both theoretical and experimental phase-shifts and backscattering amplitudes. The result of the analysis is summarized in Table I. As an example, in Fig. 6 it is shown the result of the theoretical simulation for the first coordination shell around Ce in both $CeFe_2$ and their hydride derivative at the highest hydrogen concentration. In all the cases, the hydrides exhibit a drastic reduction of the number of transition metal atoms around the rare earth site and at the same time the interatomic R-M distance are found to increase. Moreover, no evidence of R-R coordination has been detected.

Our results can only be explained by the developping of an amorphization process induced upon H_2 uptake in all the compounds investigated, in agreement to previous experimental reports [32,33,56–58,62,64–66] and in clear opposition to the crystallographic characterization reported by Tessema and coworkers [48–50], who hold the crystallinity of the hydride phases for both $CeRu_2$ and $LaRu_2$ compounds.

These findings have been discussed in the framework of the Shoemanker's occupational model to conclude that only the $A2B2$ sites are occupied [55]. However this assignment is not without controversy itself because this model indicates that the largest hydrogen absorption preserving the spatial group, is obtained by filling only the $AB3$ positions, that leads to the formula RM_2H_4. Moreover, for higher hydrogen occupancies, as those reported by Tessema and coworkers, a lowering of the crystal symmetry is expected, contrary to the reported results. However, it should be noted that the diffraction pattern reported in Ref. 50 exhibits both a non-uniform background and a considerable broadening of the diffraction lines. Although this behavior was initially associated to the existence of short-order correlation between deuteride atoms and to the fragmentation of the material, respectively [50], when associated to the posterior detection of phases containing non-hydrurated $CeRu_2$ grains [51], it strongly suggests that the materials used contained a mixed phase of crystalline-$CeRu_2$ and amorphous-$CeRu_2H_x$, thus giving rise to the controversial results discussed above.

IV. IRON K-EDGE XANES SPECTRA

The normalized XANES spectra recorded at the Fe K-edge in the case of CeFe$_2$ and CeFe$_2$H$_{3.75}$ are shown in Fig. 7. In the case of pure CeFe$_2$ the XANES spectra presents a step-like feature at the edge, characteristic of iron metal, reflecting the hybridization between the Fe $p - d$ conduction empty states at the Fermi level [11,77]. In the case of the hydrides, this feature is reduced and the threshold shifts towards higher energies. This modification is responsable of the first peak in the difference of the two XANES spectra shown in Fig. 7. The second peak, centered at about 15 eV above the absorption edge, lies in the multiple-scattering region of the spectrum in which the photoelectron is scattered in the real space by neighboring atoms, so that its origin can be addressed to the structural distortion of the atomic cluster around the iron atoms, and as determined by EXAFS analysis in the precedent section. On the contrary, in the near-edge region, extending over the first 10 eV above the threshold, the photoelectron is elastically scattered by the valence electrons and consequently, this part of the spectrum carries information about the electronic state of the absorbing atom. Indeed, the final states of the photoelectron are described as unoccupied states close to the Fermi level and, because in metals the core-hole in the final state potential is fully screened by the valence electrons close to the Fermi level, the edge spectrum esentially probes the unoccupied ground-state local and partial density of states [77]. Thus, the differences found in the near-edge region between CeFe$_2$ and CeFe$_2$H$_x$ reveal the existence of a large electronic perturbation of the system under the hydrogen absorption process: the shift of the Fe K-edge threshold observed for the hydrides can be related to the shift of the Fermi level towards higher energy, while the decrease of the intensity of the shoulder-like feature at the raising edge indicates that the density of empty $p(d)$ states above the Fermi energy decreases upon the H$_2$ uptake. Indeed, the resonance originated by the large $p - d$ hybridization of the conduction bands at the Fermi level is a probe of the density of the delocalized p-like final states.In the hydrides, the observed reduction indicates that the local density of $p(d)$-states, projected on the Fe sites, is reduced after the hydrogen absorption.

These results provide a deeper insight on the origin of the modification of the magnetic properties induced by hydrogen. In particular, they allow us to discern among the different hypothesis formulated to account for such increase in R-Fe intermetallics. The hydrogen-induced formation of low-energy electron states which are filled by electrons coming from the 3d band is one of the mechanisms invoked in the past [78] to account for the increase of μ_{Fe}, that should be due to the increase of the splitting of the 3d-band and the concomitant decrease of the Fermi energy of the systems. This is in disagreement with the observed shift towards higher energy of the Fermi level. In other related R-Fe systems, the increase of the Fe magnetic moment has been associated to the narrowing of the 3d-band due to the crystal cell expansion induced by hydrogen [4]. However, within this framework when an amorphization process takes place and the interatomic Fe-Fe distances decrease, both the widening of the 3d band and the decrease of the magnetic moment should be expected, contrary to the observed results that show a behavior of the Fe K-edge XANES similar to that previously reported for crystalline hydride phases [11,72]. This result addresses the increase of the Fe magnetic moment in these materials to the interplay between the filling of the 3d-band due to hydrogen-induced charge-transfer phenomena [79] and a weakening of the rare-earth and iron conduction bands hybridization. Moreover, both the shift of the absorption threshold and the reduction of the near-edge resonance for the $CeFe_2H_x$ are comparable to those observed for $RFe_{11}Ti$, R_2Fe_{17} and $R_2Fe_{14}B$ hydrides [11,72], in which μ_{Fe} increases slightly upon hydriding as also occurs in the RFe_2 series with the exception of $CeFe_2$. For this system the saturation magnetization of the hydride corresponds to 2.1 μ_B per Fe atom, 70% higher than in $CeFe_2$, whereas the increase is only of about the 25% for YFe_2 [3]. Therefore, a larger difference in the XANES profile for the $CeFe_2$ systems should be expected, contrary to the experimental observation. However, it should be noted that the determination of the μ_{Fe} increase upon H_2 uptake has been derived in previous reports by considering that Ce is non-magnetic in both pure $CeFe_2$ and their hydrides [80–82]. Our results can be interpreted as a first indication of a change of the electronic state of Ce to account for such an anomalous behavior, as should be discussed in the next section.

V. RARE-EARTH L_3- AND L_1-EDGE XANES SPECTRA

Attempts to understand the modification of the magnetic properties of $CeFe_2$ and $CeRu_2$ upon hydriding have been limited to the analysis of the change of valency of Ce. However, as far as many experimental techniques have been used to determine the valence of $CeRu_2$ and $CeFe_2$, offering the whole variety of results, little work has been done on the hydrides. In the case of $CeRu_2$ Bremsstralung isochromat spectroscopy measurements were initially interpreted in terms of nearly tetravalent $4f^0$ configuration [83], consistent with the 3.9 value for the Ce valence assigned indirectly through a superconductivity study of $(Ce,Th)Ru_2$ and $(La,Th)Ru_2$ compounds [42] or with that derived from lattice parameter analyses [84]. However, x-ray photoelectron spectroscopy (XPS) indicated a valence of 3.2 [85] while from Ce L_3-edge XAS data a value of 3.3 has been derived for both $CeRu_2$ [62,72,86–88] and $CeFe_2$ [62,72,86–88,91].

In the case of the $CeFe_2$ hydrides, the magnetic $4f^1$ configuration was initially assigned to Ce ions on the basis of the spectacular change of the magnetic properties occurred upon hydriding [34], whereas Deryagin et al. have reported the transition from mixed-valence to non-magnetic state, i.e., $4f^0$ configuration, based on magnetostriction and effective field analyses [82]. The same controversy holds in the case of the $CeRu_2$ system. Earlier works concluded the change of valence of Ce ions upon H_2 uptake, thus the hydrides become fully trivalent cerium compounds, because of the loss of the superconductor properties of the system. [48–51] However, this assignment has been questioned either from XAS [62,72,88] and XPS [92] experiments that although indicating the reduction of the Ce valence, show the persistence of the mixed-valence state and excluding the presence of a localized magnetic moment at the Ce sites upon hydrogen absorption.

In this section we present a systematic analysis of the Ce L_3-edge absorption spectra performed in both $CeFe_2H_x$ and $CeRu_2H_x$ at different hydrogen concentrations. This study will allow us to verify the limits of the different assignments reported in the past for the electronic state of Ce in these alloys. Moreover, the analysis of the rare earth L_1-edge

spectra in all the systems under study will provide a deeper insight on the origin of the changes occurred upon gas charging that will be discussed within a common framework.

The XANES spectra at the Ce L_3-edge for all the compounds investigated are displayed in Fig. 8. Both $CeFe_2$ and $CeRu_2$ exhibit the double-peak profile characteristic of mixed-valence Ce-based systems, i.e., there is a mixing of the $4f^0$ and $4f^1$ in the initial state. This shape reflects the superposition of the atomic $2p \rightarrow 5d$ transition for each ground state configuration, being that of the $4f^1$ configuration shifted to lower energy as compared to the $4f^0$ one because of the screening of the additional $4f$-electron [93]. Estimates of the Ce electronic valence have been done by evaluating the relative weighting of the white-line intensity associated to each ground state configuration. To this end, a deconvolution process of the normalized XANES spectra has been performed by using a least square fitting procedure. The model, discussed in detail in Ref. 11, uses arctangent functions to describe the transitions into the continuum states and Lorentzian functions to account for the atomic-like $2p \rightarrow 5d$ transitions.

The deconvolution of the L_3 absorption edge of cerium for $CeFe_2$ and $CeRu_2$ returns a valence of 3.29 and 3.30 respectively. Upon hydrogen absorption, the modification of the XANES profile for both compounds is quite different. Indeed, in the case of the $CeFe_2$ hydrides the double-peak structure characteristic of mixed-valence behavior disappears and only the white-line corresponding to the $4f^1$ configuration, i.e., magnetic Ce, is evidenced. On the contrary, the experimental spectra of the $CeRu_2$ hydrides still exhibit the presence of the two configurations although a significant decrease of the $4f^0$ component takes place. In this way, the least square fitting returns a Ce valence of 3 for all the $CeFe_2$ hydrides investigated, whereas for $CeRu_2H_{2.9}$ and $CeRu_2H_{4.8}$ the Ce valence is found to be 3.08 and 3.12 respectively. The Ce mixed-valence behavior is retained in all the Ru-based systems, ruling out the possibility that the loss of superconductivity is associated to the developing of a $4f$ magnetic moment induced by hydrogen uptake. From our XAS data, the magnetic properties of the $CeFe_2$ hydrides appear linked to the modification of the Ce electronic state. Indeed, if we use a molecular field model to describe the variation of the magnetic ordering

temperature in the RFe_2 series, T_c can be written as [96]

$$3kT_c = a_{FeFe} + a_{RR} + \left[(a_{FeFe} - a_{RR})^2 + 4a_{FeR}a_{RFe}\right]^{\frac{1}{2}} \tag{2}$$

where a_{xy} represent the magnetic interaction energy between the x and y spins. Neglecting the relative weak R-R exchange energy, this expression reduces to

$$3kT_c = a_{FeFe} + \left[a_{FeFe}^2 + 4a_{FeR}a_{RFe}\right]^{\frac{1}{2}} \tag{3}$$

These energies can be expressed in terms of the coupling constants J_{RFe} and J_{FeFe} by means of the relations

$$a_{FeFe} = Z_{FeFe}J_{FeFe}S_{Fe}(S_{Fe} + 1) \tag{4}$$

$$a_{RFe}a_{FeR} = Z_1 Z_2 S_{Fe}(S_{Fe} + 1)J_{RFe}^2(g_J - 1)^2 J(J + 1) \tag{5}$$

where Z_{FeFe} is the average number of similar atoms around one Fe atom, and Z_1 and Z_2 are respectively the number of Fe neighbors of a R atom and the number of R neighbors around an Fe atom. Substituting in Eq. 3 the experimental value of T_c of the YFe_2 compound it is possible to determine the value of the J_{FeFe} coupling constant. Then, with this value and the experimental data of $GdFe_2$ it is possible to estimate J_{RFe}. These values have been used to calculate the magnetic ordering temperature for all the RFe_2 series, as reported in Table II. Now, if we consider that Ce ions are present in the $4f^1$ configuration in $CeFe_2$, we obtain a T_c value of 544 K, that is comparable to those of the rest of the series but more than twice the experimental value. This is in excellent agreement with the mixed-valence behavior determined by XANES analysis. Moreover, according to the value of T_c calculated for an hypothetical Ce^{3+} $CeFe_2$ compound, T_c is found to decrease upon hydrogen uptake in the same manner and with the same magnitude as for the whole RFe_2 series. If necessary, this result is an additional verification of the stabilization of a localized 4f magnetic moment upon hydrogen absorption in the $CeFe_2$ system.

Regarding the behavior of the $CeRu_2$ hydrides, our data show the existence of the mixed-valence behavior also after the hydrogen uptake. Thus, the results derived from our Ce

L_3-edge analysis clarify both the mechanism responsible for the superconductivity in these alloys, and the reason why this property is loss upon H_2 uptake. Because hydrogen absorption leads to the disapparition of the superconductivity in $CeRu_2$, several authors addressed the localization of a 4f magnetic moment on the Ce sites taking place during the absorption process [48–51]. However, if one considers that superconductivity is avoided by the localization of the Ce magnetic moment, the question arising immediately is why the same behavior occurs for the $LaRu_2$ hydrides, in which no 4f electrons are present.

The comparison of the superconductivity properties of both $LaRu_2$ and $CeRu_2$ systems as well as their response to different substitutions at both the Ru and rare-earth sites, led to the assignment of superconductivity to Ru-4d bands in both compounds [42–44]. Recent theoretical band calculations have confirmed the critical role of the d electrons of Ru [97], while other calculations have assigned the superconductivity to the Ce 4f localized electrons [45,46]. However, because our results at the Ce L_3-edge do not support this last possibility, and trying to solve the puzzle, we have also studied the XANES spectra at the L_1-edge of the rare-earth (La and Ce) in both $LaRu_2$, $CeRu_2$ and their hydrides derivatives.

The spectral shape of the L_1 spectra in all the lanthanide metals exhibits a step-like rise of the absorption at the threshold. This feature reflects the p-projected density of states in the band structure of the conduction electrons. In the case of rare-earths vapors, such a structure is absent in the L_1 spectra because the atomic resonances corresponding to the one-electron transition $s - p$ are very weak due to the small oscillator strengths of the $s - p$ transitions [98,99]. However, upon condensation into the metallic state, the L_1 spectra loss their atomic character completely and a shoulder-like feature appears. [100] This behavior is the experimental evidence that the outer p-symmetry orbitals are strongly hybridized with the outer s- and d-symmetry orbitals in metals, reflecting the high density of empty 5d states via hybridization of the R(sp) and R(5d) empty states. Therefore, the modification of the width and intensity of the shoulder-like near-edge structure is a fingerprint of hybridization changes of the outermost orbitals between the absorbing atom and the nearest neighbors [101]. In particular, in the case of R-M intermetallic compounds,

due to the strong hybridization between the rare earth and transition metal d orbitals, the study of the L_1 absorption spectra provide an unique insight to study the behavior of the R-M hybridization upon gas charging.

Fig. 9 shows the comparison of the XANES spectra at the Ce L_1-edge in both $CeFe_2$ and $CeRu_2$ and their hydrides derivatives. In both cases, a reduction of the shoulder-like feature is induced by hydrogen absorption, indicating a more localized nature of the $p - d$ orbitals of the rare-earth, similar to the rare-earth vapors case. This result supports the hypothesis that a higher localization of the $5d$ band at the rare earth site takes place upon hydriding, as well as the concomitant reduction of the $Ce(5d)$-$Fe(3d)$ and $Ce(5d)$-$Ru(4d)$ overlap that determines the interplay between the two magnetic sublattices. It is important to note that the same result is found in both cases, independently of the developping of 4f magnetic moment at the Ce sites occurring in the $CeFe_2$ hydrides and that does not take place in the $CeRu_2$ hydrides. This interpretation is supported by the result found for the La L_1-edge XANES spectra in the case of $LaRu_2$ and their hydrides, exhibiting the same behavior, as shown in Fig. 10. These results indicate the main role played by the modification of the La-Ru hybridization induced by hydrogen absorption into driving the changes of the magnetic behavior in the hydrides. All these results are in complete agreement with the assignment that identifies the Ru-$4d$ band as the responsible for the superconductivity in these systems.

VI. CONCLUSIONS

In this work we have presented the analysis of the XAS spectra recorded at the Fe K-edge and at the rare-earth L_3-edge in the C15 Friauf-Laves $CeFe_2$, $CeRu_2$ and $LaRu_2$ and their hydrides at different hydrogen concentrations.

EXAFS investigation determines unambiguously that hydrogen leads to the amorphization of the three systems. Moreover, the capability of the EXAFS technique to test the local atomic sites has allowed us to determine for the first time the local environment around the rare earth and the transition metal independently. The comparison with theoretical compu-

tations determines the new coordination numbers around each atomic species as well as the interatomic distances to the nearest neighbors, remaining after the amorphization process.

Once the structural changes occurred upon hydriding has been clarified, we analyzed their correlation with the modification of the electronic and magnetic properties of these systems. In particular, from the analysis of the Ce L_3-edge we demonstrate the change of Ce valence in $CeFe_2$ upon H_2 uptake, in such a way that a localized Ce $4f$ magnetic moment is developed in their hydrides, while, contrary to previous assignments, Ce still remains in a mixed valence state in the $CeRu_2$ hydride derivatives.

In addition, in the case of $CeFe_2$, the combined analysis of the Fe K-edge and Ce L_1-edge XANES spectra shows strong electronic effects induced upon H_2 uptake, addressing the enhancement of the Fe magnetic moment to the interplay between electronic charge transfer to the conduction bands and the weakening of the hybridization between the Ce $5d$- and the Fe $3d$-states.

The same analysis have been performed in the case of $LaRu_2$ and $CeRu_2$. In the case of the $CeRu_2$ hydrides our results exclude the promotion of a localized $4f$ magnetic moment induced by hydrogen absorption as the origin of the modification of the magnetic properties. On the contrary, the present XAS data demonstrate the key role played by the hybridization of the f states with other extended states into determining the magnetic behavior of $CeRu_2$ and its related materials, as recently predicted by theoretical electronic-structure calculations [102]. Indeed, the loss of the supeconductivity behavior upon hydriding in these systems, has been succesfully discussed in the present work in a common framework in which the strong structural modification as well as the decrease of the $4d(Ru) - 5d(Ce, La)$ hybridization, are identified as the responsible for the change of the magnetic behavior.

ACKNOWLEDGMENTS

REFERENCES

[1] H.H. van Mal, Philips Res. Repts. Suppl. 1, 1 (1976).

[2] K.H.J. Buschow, P.C.P. Bouten and A.R. Miedema, Rep. Prog. Phys. 45, 937 (1982) and references therein.

[3] W.E. Wallace, in *Hydrogen in Metals* Vol. I, edited by G. Alefeld and J. Volkl, Topics in Applied Phys. Vol. 28 (Springer-Verlag, Berlin, 1978) and references therein.

[4] K.H.J. Buschow, in *Handbook on the Physics and Chemistry of Rare Earths*, edited by K.A. Gschneidner Jr. and L. Eyring, Vol. 6, (North-Holland, Amsterdam, 1984) and references therein.

[5] G. Wiesinger and G. Hilscher, in *Handbook of Magnetic Materials*, edited by K.H.J. Buschow, Vol. 6, (Elsevier, Amsterdam, 1991) and references therein.

[6] M. Yamaguchi and E. Akiba, in *Materials Science and Technology*, edited by R.W. Cahn, P. Haasen and E.J. Kramer, Vol. 3B, (VCH, Weinheim, 1994) and references therein.

[7] O. Eriksson, L. Nördstrom, M.S.S. Brooks and B. Johansson, Phys. Rev. Lett. 60, 2523 (1988).

[8] L. Nördstrom, O. Eriksson, M.S.S. Brooks and B. Johansson, Phys. Rev. B41, 911 (1990).

[9] O. Eriksson, M.S.S. Brooks and B. Johanson, Phys. Rev. B 41, 7311 (1990)

[10] B. Johanson, L. Nordström, O. Eriksson and M.S.S. Brooks, Physica Scripta T39, 100 (1991).

[11] J. Chaboy, A. Marcelli, L. Bozukov, F. Baudelet, E. Dartyge, A. Fontaine and S. Pizzini, Phys. Rev. B 51, 9005 (1995).

[12] K.H.J. Buschow, J. Less Common Met. 51, 1977 (1973).

[13] J. Farrel and E. Wallace, J. Chem. Phys. **41**, 1924 (1964).

[14] K.H.J. Buschow and I.S. van Wieringen, Phys. Status Solidi **42**, 231 (1970).

[15] M. Rosen, H. Klimer, U. Atzmony and M. P. Dariel, Phys. Rev. B **9** 254 (1974).

[16] U. Atzmony and M. P. Dariel, Phys. Rev. B **10**, 2060 (1974).

[17] H.R. Kirchmayr and C.A. Poldy, in *Handbook on the Physics and Chemistry of Rare Earths*, edited by K.A. Gschneidner Jr. and L. Eyring, Vol. 2, (North-Holland, Amsterdam, 1979) and references therein.

[18] S.F. Da Cunha, D.F. Franceschini, S. Senoussi and A. Y. Takeuchi, J. Phys. F **12**, 3083 (1982).

[19] D.F. Franceschini and S.F. Da Cunha, J. Mag. Magn. Mater. **52**, 280 (1985).

[20] S.B. Roy and B.R. Coles, J. Phys. F **17**, L215 (1987).

[21] Y. Nishihara, M. Tokumoto, Y. Yamaguchi and G. Kido, J. Mag. Magn. Mater. **70**, 173 (1987).

[22] S.B. Roy and B.R. Coles, J. Phys. Condens. Matter **1**, 419 (1989).

[23] P.N. Tandon, R.G. Pillay, A.K. Grover and V. Balasubramanian, Hyperfine Interact. **50**, 733 (1989).

[24] S.B. Roy and B.R. Coles, J. Appl. Phys. **63**, 4094 (1988).

[25] S.J. Kennedy, A.P. Murani, B.R. Coles and O. Moze, J. Phys. F **18**, 2499 (1988).

[26] S.J. Kennedy, A.P. Murani, J.K. Cockcroft, S.B. Roy and B.R. Coles, J. Phys. Condens. Matter **1**, 629 (1989).

[27] S.B. Roy and B.R. Coles, Phys. Rev. B **39**, 9360 (1989).

[28] S.J. Kennedy and B.R. Coles, J. Phys. Condens. Matter **2**, 1213 (1990).

[29] S.B. Roy, G. Williams and B.R. Coles, J. Physique **50**, 2733 (1989).

[30] P.K. Khowash, Phys. Rev. B **43**, 6170 (1991).

[31] P.K. Khowash, Physica B **163**, 197 (1990).

[32] K.H.J. Buschow, Solid State Commun. **19**, 421 (1976).

[33] A.M. van Diepen and K.H.J. Buschow , Solid State Commun. **22**, 113 (1977).

[34] K.H.J. Buschow and A.M. van Diepen, Solid State Commun. **19**, 79 (1976).

[35] A.V. Deryagin, A.A. Kazakov, N.V. Kudrevatykh, V.N. Moskalev, N.V.Mushnikov and S.V. Terent'yev, Phys. Met. Metall. **60**, 81 (1985).

[36] B. T. Matthias, H. Shul and E. Corenzwit, Phys. Rev. Lett **1**, 449 (1958).

[37] B. Hillebrand and M. Wilhelm, Phys. Letters A **31**, 448 (1970).

[38] M. Wilhelm and B. Hillebrand, Z. Naturforsch A **26**, 141 (1971).

[39] B. Hillebrand and M. Wilhelm, Phys. Letters A **33**, 61 (1970).

[40] M. Wilhelm and B. Hillebrand, Physica **55**, 608 (1971).

[41] M.B. Maple, Appl. Phys. **9** , 179 (1976) and references therein.

[42] M. Hakimi and J. G. Huber, Physica B **135**, 434 (1985).

[43] C. Rettori, D. Davidov, P. Chaikin and R. Orbach, Phys. Rev. Lett. **30**, 437 (1973).

[44] K.H. Bennemann and J.W. Garland, Inter. J. Mag. **1**, 97 (1971).

[45] A. Yanase, J. Mag. Magn. Mat. **31**, 453 (1983).

[46] A. Yanase, J. Phys. F **16**, 1501 (1986).

[47] P. de V. du Plessis, Physica B **163**, 603 (1990).

[48] G. X. Tessema, J. Peyrad, A. Nemoz, J.P. Senateur, A. Rouault and R. Fruchart, J.

de Physique **40**, L105-107 (1979).

[49] D. Fruchart, F. Vaillant, E. Roudaut, A. Nemoz and X.G. Tessema, Phys. Stat. Sol (a) **65**, K19 (1981).

[50] D. Fruchart, F. Vaillant, A. Rouault, A. Benoit and J. Flouquet, J. Less-Common Met. **101**, 285 (1984).

[51] S. Miraglia, M. Anne, H. Vincent, D. Fruchart, J. M. Laurant and M. Rossignol, J. Less-Common Met. **153**, 51 (1989).

[52] See for example, D.E. Sayers and B.A. Bunker, in *X-ray Absorption: Principles, Applications, Techniques of EXAFS, SEXAFS and XANES*, edited by D.C. Koningsberger and R. Prins, (John Wiley Sons, New York, 1988) Chap. 6.

[53] B. Lengeler and P. Eisenberger, Phys. Rev. B **21**, 4507 (1980).

[54] A. Pebler and E.A. Gulbransen, Trans. Metall. Soc. AIME **239**, 1593 (1967).

[55] D. P. Shoemaker and C. B. Shoemaker, J. Less-Common Met. **68**, 43 (1979).

[56] K. Aoki, T. Yamamoto, Y. Satoh, K. Fukamichi and T. Masumoto, Acta Metall. **35**, 2465 (1987).

[57] J. Chaboy, J. García, A. Marcelli and M.F. Ruiz Lopez, Chem. Phys. Lett. **174**, 389 (1990).

[58] Y.-G. Kim and J.-Y. Lee, J. Alloys and Comp. **187**, 1 (1992).

[59] K. Aoki, T. Yamamoto and T. Masumoto, Scripta Metall. **21**, 27 (1987).

[60] V. Paul-Boncour, A. Percheron-Guegan, M. Diaf and J.C. Archad, J. Less-Common Met. **131**, 201 (1987).

[61] N. Kataoka, X.-G. Li, K. Aoki and T. Masumoto, J. Less Common Met. **162**, L11 (1990).

[62] J. García, A. Marcelli, M. Sanchez del Rio, J. Bartolomé, D. Fruchart, S. Miraglia and F. Vaillant, Physica B **158**, 521 (1989).

[63] J. García, J. Bartolomé, M. Sanchez del Rio, A. Marcelli, D. Fruchart and S. Miraglia, Z. Phys. Chem. **163**, 277 (1989).

[64] P. Raj, P. Suryanarayana, A. Sathyamoorthy, K. Shashikala, K.V. Gopalakrishnan and R.M. Iyer, J. Alloys and Comp. **179**, 99 (1992).

[65] Y.-G. Kim, U.-I. Chung and J.-Y. Lee, J. Alloys and Compounds **202**, 203 (1993).

[66] Y.-G. Kim and J.-Y. Lee, Scripta Metall. et Mater. **24**, 2123 (1990).

[67] P.A. Lee and G. Beni, Phys. Rev B **15**, 2862 (1977).

[68] Note that the phase correction was not included in the Fourier transform, therefore the peak positions are shifted from their true values. C.A. Ashley and S. Doniach, Phys. Rev. B **11**, 1279 (1975).

[69] N. Binsted, S.J. Gurman and S. Campbell, SERC Daresbury Laboratory, (unpublished).

[70] S.J. Gurman, N. Binsted and I. Ross, J. Phys. Condens. Matt. **7**, 143 (1984).

[71] *Report of the International Workshop on Standards and criteria in X-ray Absortion Spectroscopy*, Physica B **158**, 701 (1989).

[72] J. Chaboy, Ph. D. Thesis, Zaragoza University, (1991).

[73] J. Chaboy and T.A. Tyson, Phys. Rev. B **49**, 5869 (1994).

[74] J. Chaboy, A. Marcelli and T.A. Tyson, Phys. Rev. B **49**, 11652 (1994).

[75] J. Chaboy, T.A. Tyson and A. Marcelli, *Relative cross sections for bound-state double-electron $LN_{4,5}$-edge transitions of rare-earths and Nonradioactive elements of the sixth row.*", (Prensas Universitarias, Zaragoza, 1995).

[76] J.A. Solera, J. Garcia and M.G. Proietti, Phys. Rev. B **51**, 2678 (1995).

[77] A. Bianconi, in *X-ray Absorption: Principles, Applications, Techniques of EXAFS, SEXAFS and XANES*, edited by D.C. Koningsberger and R. Prins, (John Wiley & Sons, New York, 1988) Chap. 11 and references therein.

[78] A.V. Andreev, A.V. Deryagin, N.V. Kudrevatykh, N.V. Mushnikov, V.A. Reimer and S.V. Terent'ev, Sov. Phys. JETP **63**, 608 (1986).

[79] F.A. Kuijpers, Philips Res. Repts. Suppl. **2**, (1973).

[80] K.H.J. Buschow, Sol. State Commun. **19**, 421 (1976).

[81] K.H.J. Buschow, Physica **86-88B**, 79 (1977).

[82] A.V. Deryagin, A.A. Kazarov, N.V. Kudrevatykh, V.N. Moskalev, N.V. Mushnikov and S.V. Terent'yev, Phys. Met. Metall. **60**, 81 (1985).

[83] E. Wuilloud, Y. Baer and M.B. Maple, Phys. Lett. **97A**, 65 (1983).

[84] A. Troper, O.L.T. de Menezes and A.A. Gomes, Sol. State Commun. **38**, 831 (1981).

[85] J.C. Fuggle, F.U. Hillebrecht, Z. Zolnierek, R. Lasser, Ch. Freiburg, O. Gunnarsson and K. Schonhammer, Phys. Rev. B **27**, 7330 (1983).

[86] D. Wohlleben and J. Röhler, J. Appl. Phys. **55**, 1904 (1984).

[87] K.R. Bauchspiess, W. Boksch, E. Holland-Moritz, H. Launois, R. Pott and D. Wohelleben, in *Valence Fluctuations in Solids*, edited by L.M. Falicov, W. Hanke and M. B. Maple, (North-Holland, Amsterdam, 1981), 417.

[88] J. Chaboy, J. García and A. Marcelli, J. Magn. Magn. Mater. **104-107**, 661 (1992).

[89] J.W. Allen, S.J. Oh, I. Lindau, M.B. Maple, J.F. Suassuna and S.B. Hangstrom, Phys. Rev. B **26**, 445 (1982).

[90] J.W. Allen, S.J. Oh, M.B. Maple and M.S. Torikachvili, Phys. Rev. B **28**, 5743 (1983).

[91] R.A. Neifeld and M.A. Croft, J. Magn. Magn. Mater. **47-48**, 36 (1985).

[92] J. Osterwalder, T. Riesterer, L. Schlapbach, F. Vaillant and D. Fruchart, Phys. Rev. B **31**, 8311 (1985).

[93] S.M. Blokhin and E. Ye. Vaynshteyn, Fiz. Met. Metaloved. **19**, 371 (1965).

[94] J. Röhler, in *Handbook on the Physics and Chemistry of Rare Earths*, edited by K.A. Gschneidner Jr. and L. Eyring and S. Hufner, Vol. 10, (North-Holland, Amsterdam, 1987).

[95] J. Röhler, J. Magn. Mag. Mat. 47&48 175 (1985).

[96] See for example, K.H.J. Buschow, in *Handbook of Magnetic Materials*, edited by E.P. Wohlfarth, Vol. 4, (North-Holland, Amsterdam, 1988) and references therein.

[97] R. Asokamani, G. Subramoniam, S. Mathi Jaya and S. Pauline, Phys. Rev. B **44**, 2283 (1991).

[98] G. Materlik, J.E. Müller and J.W. Wilkins, Phys. Rev. Lett. **50**, 267 (1983).

[99] J.E. Müller and J.W. Wilkins, Phys. Rev. B **29**, 4331 (1984).

[100] G. Materlik, B. Sonntag and M. Tausch, Phys. Rev. Lett. **51**, 1300 (1983).

[101] A. Marcelli and A. Bianconi, Physica B **158**, 529 (1989).

[102] J. Costa-Quintana, E. González-León, F. López-Aguilar, L. Puig-Puig and M.M. Sánchez-López, Physica B **206&207**, 186 (1995).

TABLES

TABLE I. Coordination numbers, interatomic distances and fit-index parameters obtained from the comparison of the experimental spectra and the theoretical simulations as described in the text.

Compound	Coordination	R(Å)	FI	Coordination	R (Å) XRD
K-Fe Theoretical phases					
$CeFe_2$	6 Fe	2.51	0.64	6 Fe	2.58
	6 Ce	2.96		6 Ce	3.03
$CeFe_2H_x$	3±1 Fe	2.47	0.50		
K-Fe Experimental phases					
$CeFe_2H_x$	3±1 Fe	2.57			
	2±2 Ce	3.25			
L_3-Ce Theoretical phases					
$CeFe_2$	12 Fe	2.96	0.65	12 Fe	3.03
	4 Ce	3.12		4 Ce	3.16
$CeFe_2H_x$	3±1 Fe	3.028	0.05		
$CeRu_2$	12 Ru	3.04	0.52	12 Ru	3.12
	4 Ce	3.18		4 Ce	3.26
$CeRu_2H_x$	4±2 Ru	3.08	0.27		
L_3-Ce Experimental phases					
$CeFe_2H_x$	4±2 Fe	3.18			
$CeRu_2H_x$	4±2 Ru	3.14			
L_3-La Theoretical phases					
$LaRu_2$	12 Ru	3.08	0.64	12 Ru	3.19
	4 La	3.42		4 La	3.30
$LaRu_2H_x$	6±1 Ru	3.23	0.18		
L_3-La Experimental phases					
$LaRu_2H_x$	4±2 Ru	3.25			

TABLE II. Experimental and calculated magnetic ordering temperatures for the RFe_2 series together with the T_c values for the hydrides

Compound	RFe_2 T_c (K)	RFe_2 T_c(K) (calc.)	RFe_2H_x T_c(K)
YFe_2	545	545	308
$CeFe_2$	230	544	358
$SmFe_2$	676	627	333
$GdFe_2$	785	785	388
$TbFe_2$	711	718	303
$HoFe_2$	612	627	298
$ErFe_2$	590	592	265
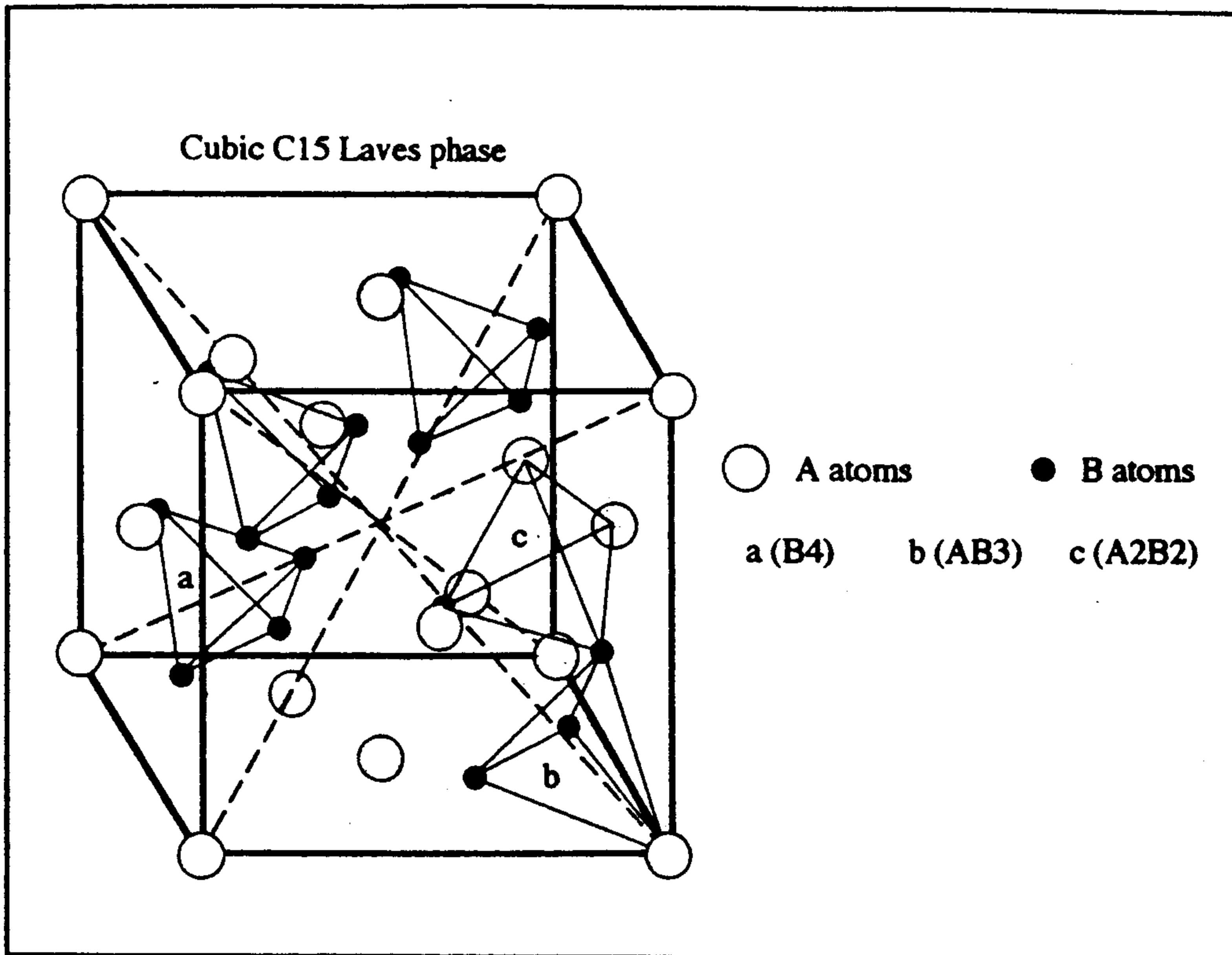
Figure 1 – Crystallographic structure of the cubic C15 Laves phase structure showing the three types of tetrahedral interstices.
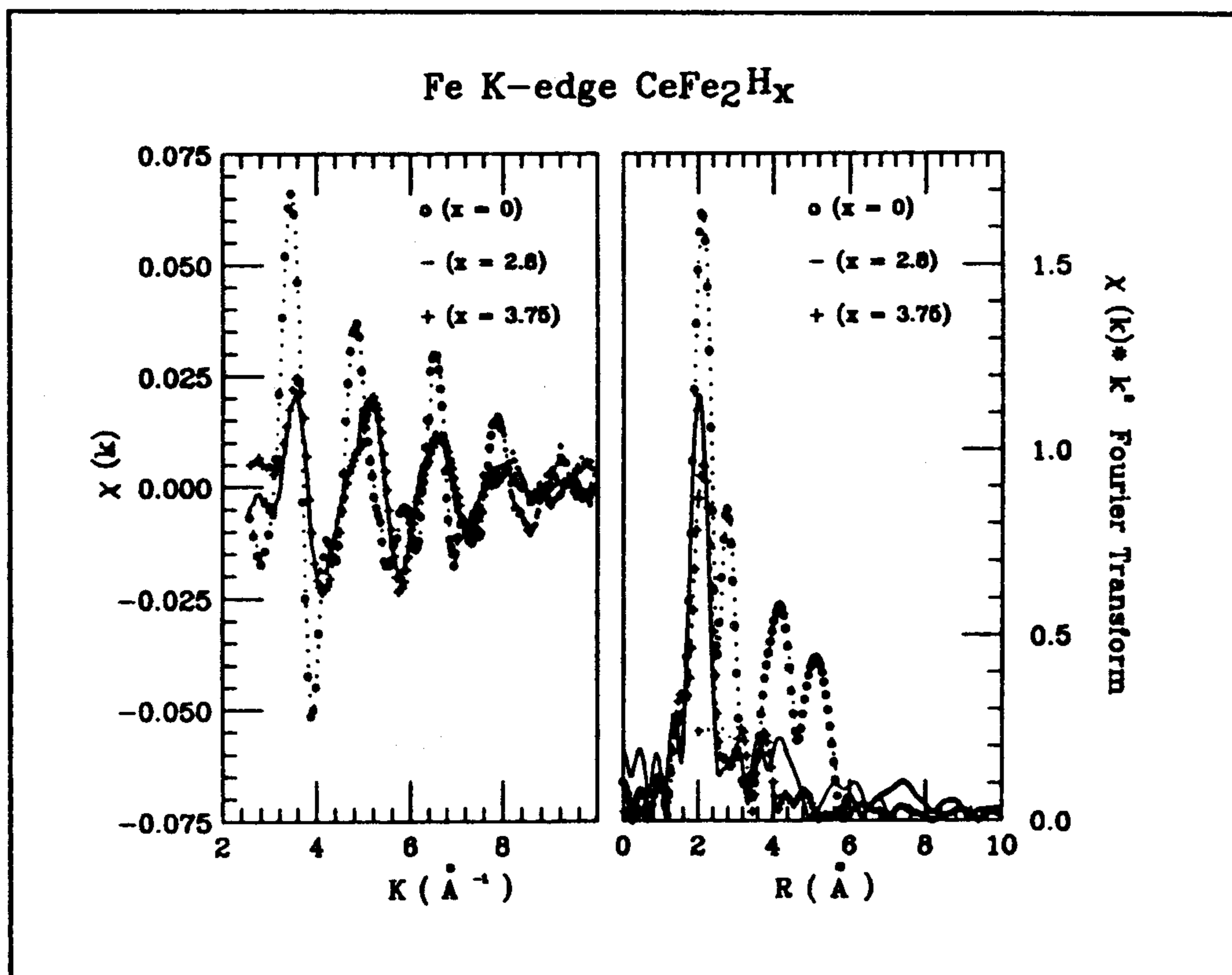
Figure 2 – Extracted iron K-edge EXAFS signals in $CeFe_2$ and their hydrides derivatives. The corresponding k^2-weighted Fourier transforms are shown in the right panel.

Fe K—edge CeFe$_2$

a)

Fe K—edge CeFe$_2$H$_{3.75}$

b)
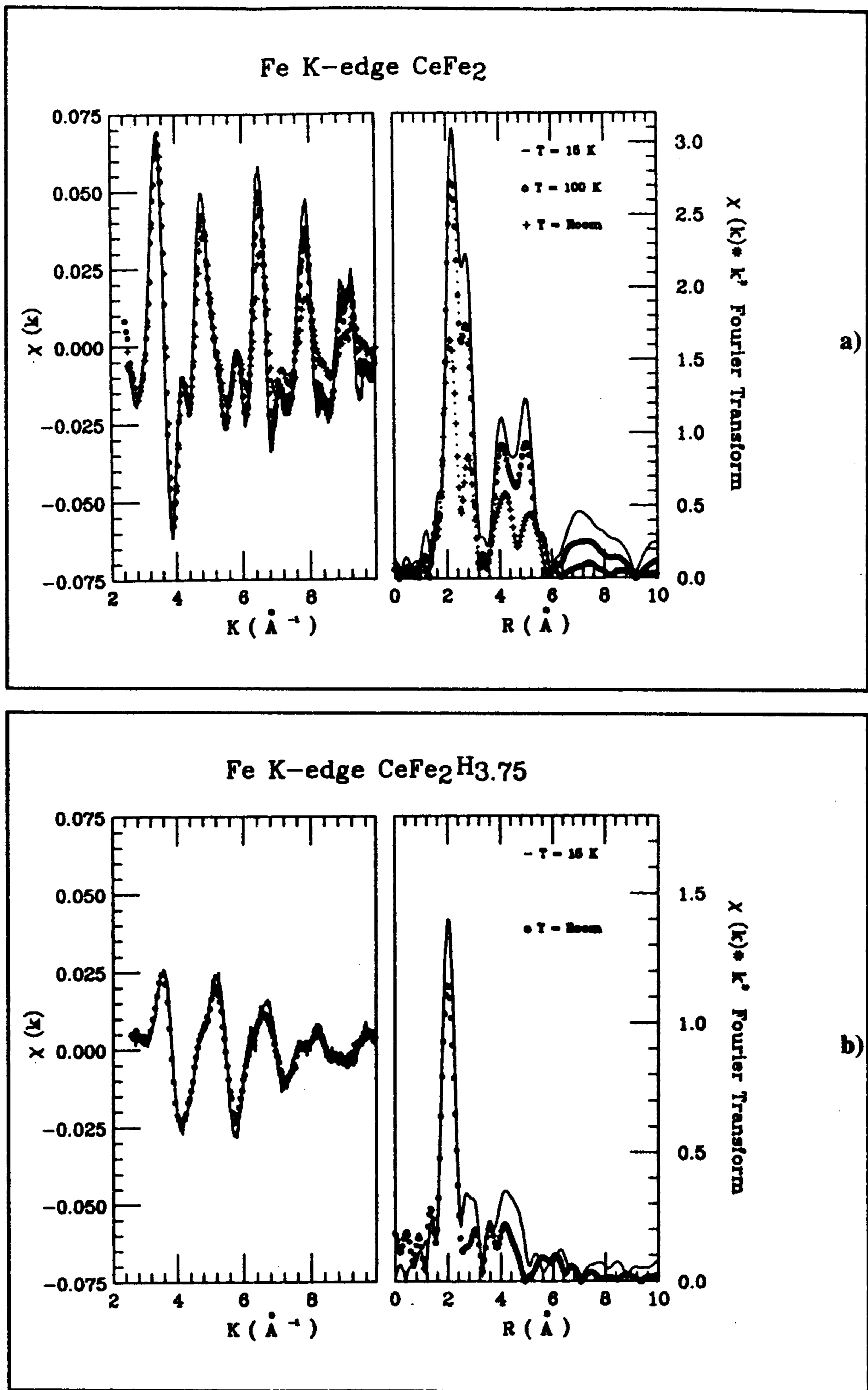
Figure 3 – Temperature dependence of the Fe K-edge EXAFS signals (left panel) and their Fourier transforms (right panel) recorded at different temperatures in a) CeFe$_2$ and b) CeFe$_2$H$_{3.75}$.
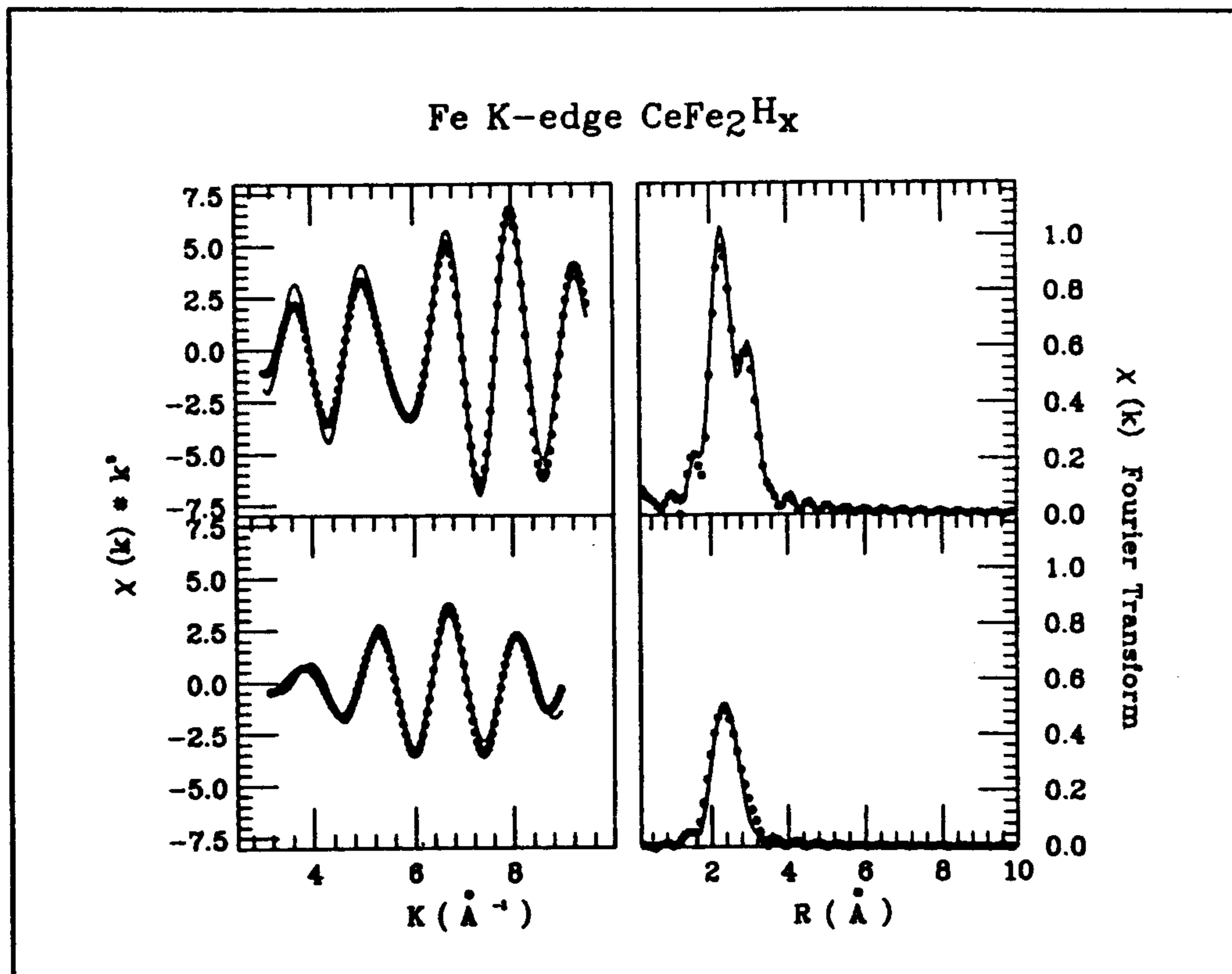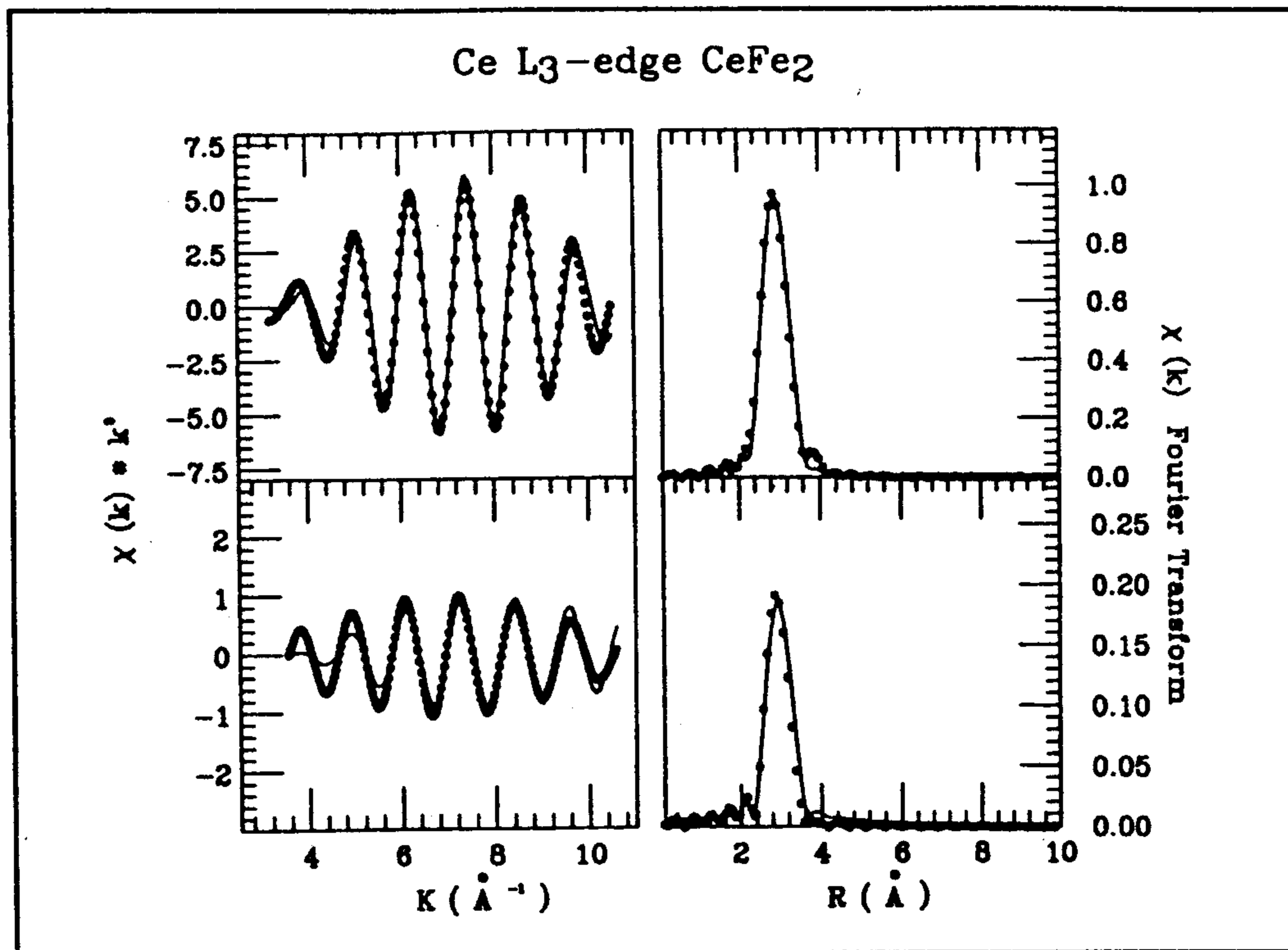
Figure 4 – Comparison between the experimental Fe K-edge filtered spectrum (dots) of CeFe$_2$ (upper panel) and CeFe$_2$H$_{3.75}$ (bottom panel) and the theoretical simulations (solid line). The same comparison on the Fourier transforms is shown in the right panel (see text for details).
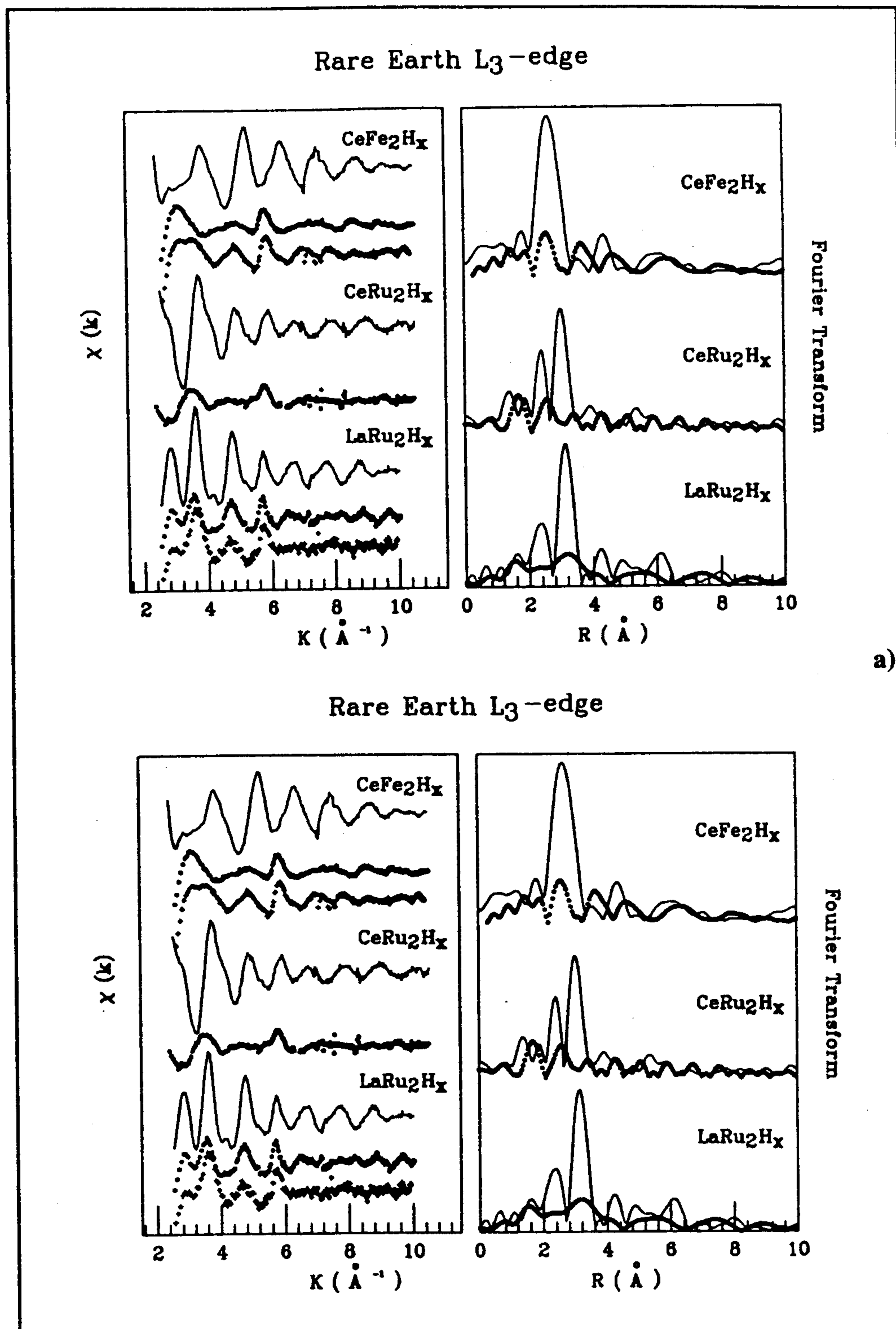
Figure 5 – a) From top to bottom, comparison of the rare earth L_3-edge EXAFS spectra of $CeFe_2H_\chi$ with x=0 (solid), 2.8 (dots) and 3.75 (+); $CeRu_2H_\chi$ with x= 0 (solid) and 4 (dots); and $LaRu_2H_\chi$ with x= 0 (solid), 2.8 (dots) and 4.8 (+). In the right panel the same comparison is shown for the Fourier transforms of the pure compounds and their hydride derivatives with the highest hydrogen content.
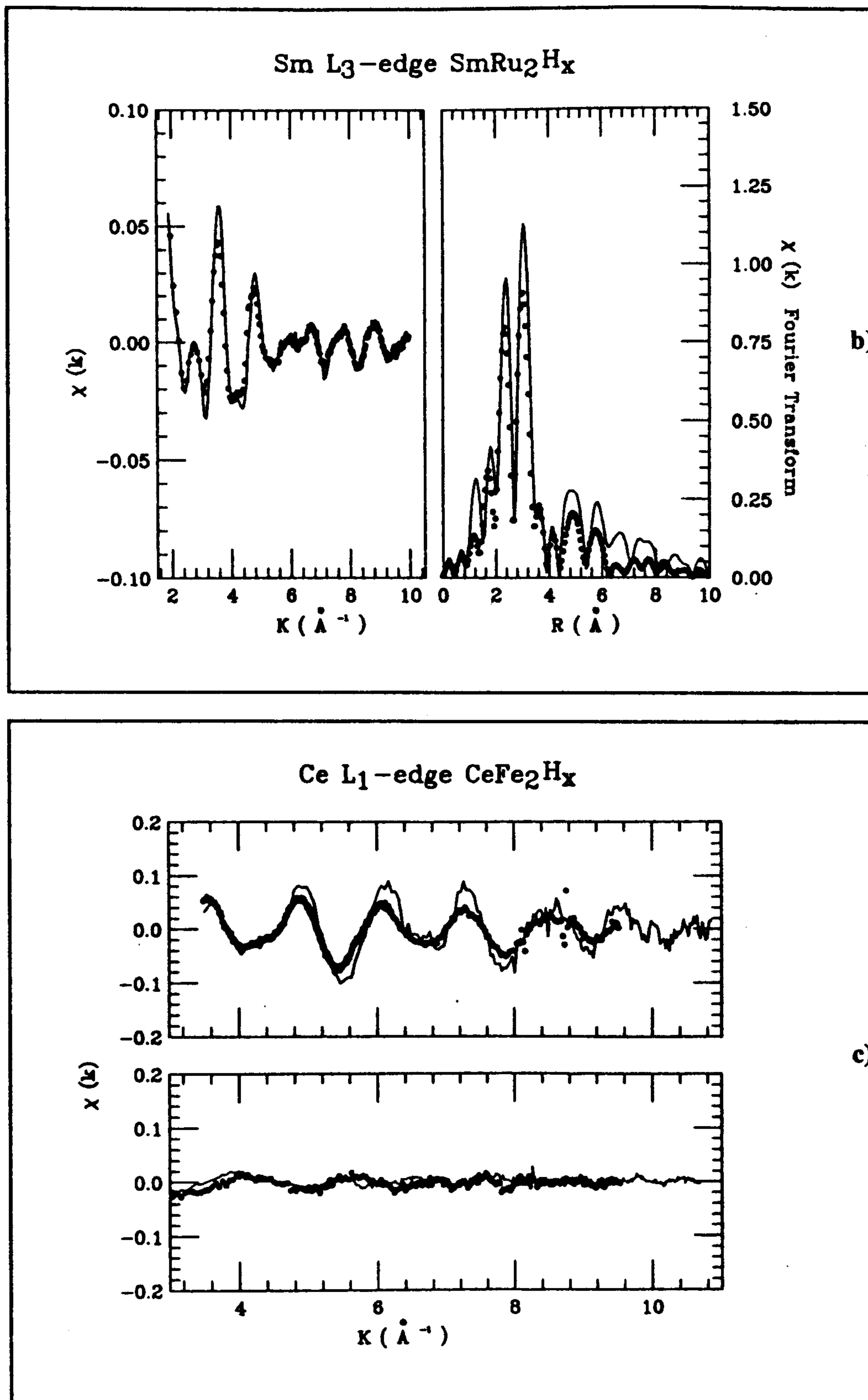
Figure 5 – (b) Comparison of the Sm L_3-edge EXAFS spectra and their Fourier tranforms in the case of $SmRu_2H_x$ with x= 0 (solid) and 4.8 (dots). c) Comparison of the Ce L_1-edge EXAFS spectra for $CeFe_2$ (top panel) and $CeFe_2H_{3.75}$ (bottom panel) recorded at room temperature (dots) and at 15 K.

Figure 6 – Comparison between the experimental Ce L_3-edge filtered spectrum (dots) of CeFe$_2$ (upper panel) and CeFe$_2$H$_{3.75}$ (bottom panel) and the theoretical simulations (solid line) described in the text. The same comparison on the Fourier transforms is shown in the right panel.
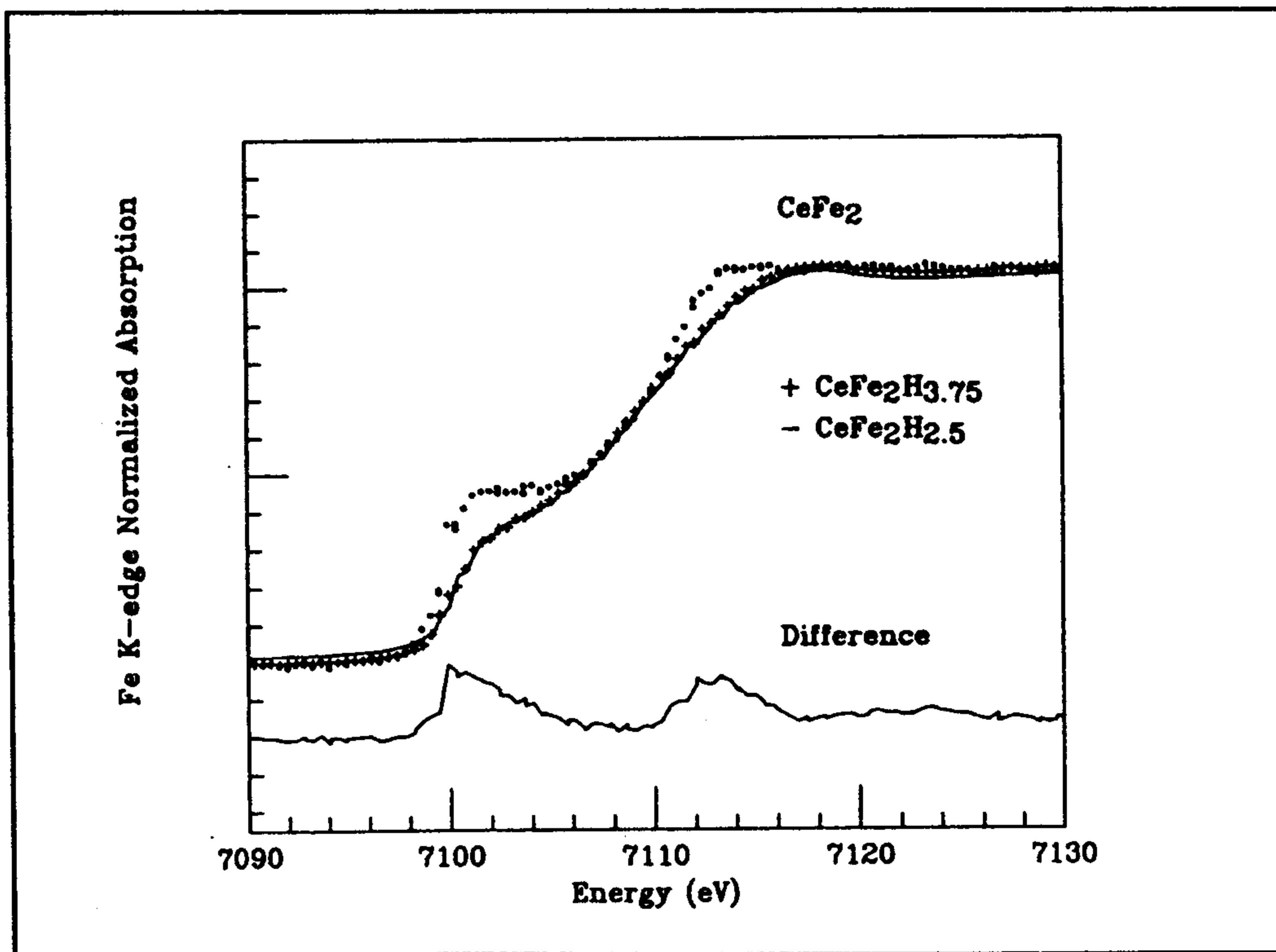
Figure 7 – Comparison between the experimental XANES spectra at the Fe K-edge in the case of CeFe$_2$ (dots), CeFe$_2$H$_{2.5}$ (solid) and CeFe$_2$H$_{3.75}$ (+). The difference spectrum in the bottom is multipled by a factor 2 (solid line).
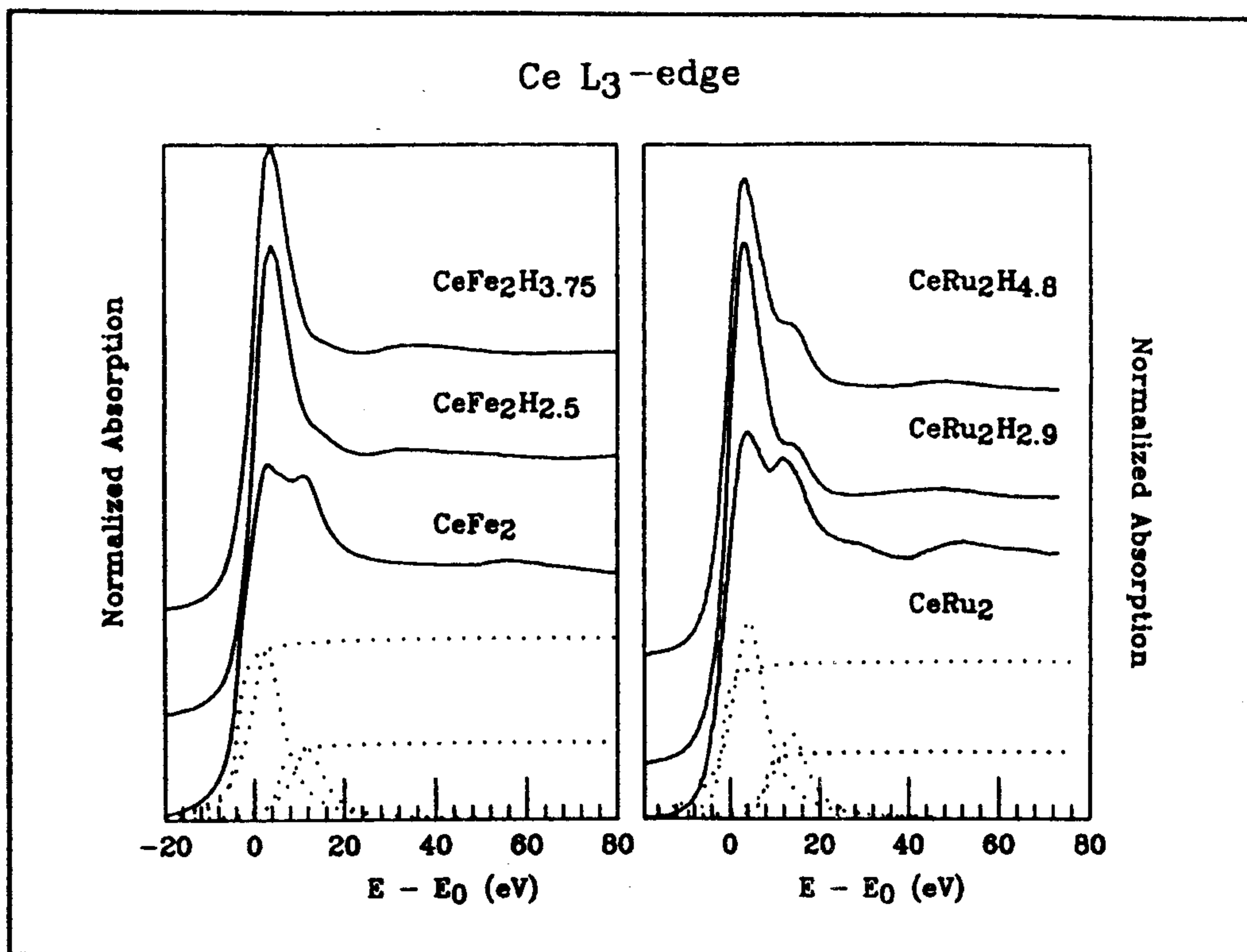
Ce L₃−edge

Figure 8 – Comparison of the Ce L_3-edge absorption spectrum in the CeFe₂Hx (left panel) and CeRu₂H$_x$ (right panel) systems at different hydrogen concentration. The deconvolution of the spectra for the pure compounds is also shown.
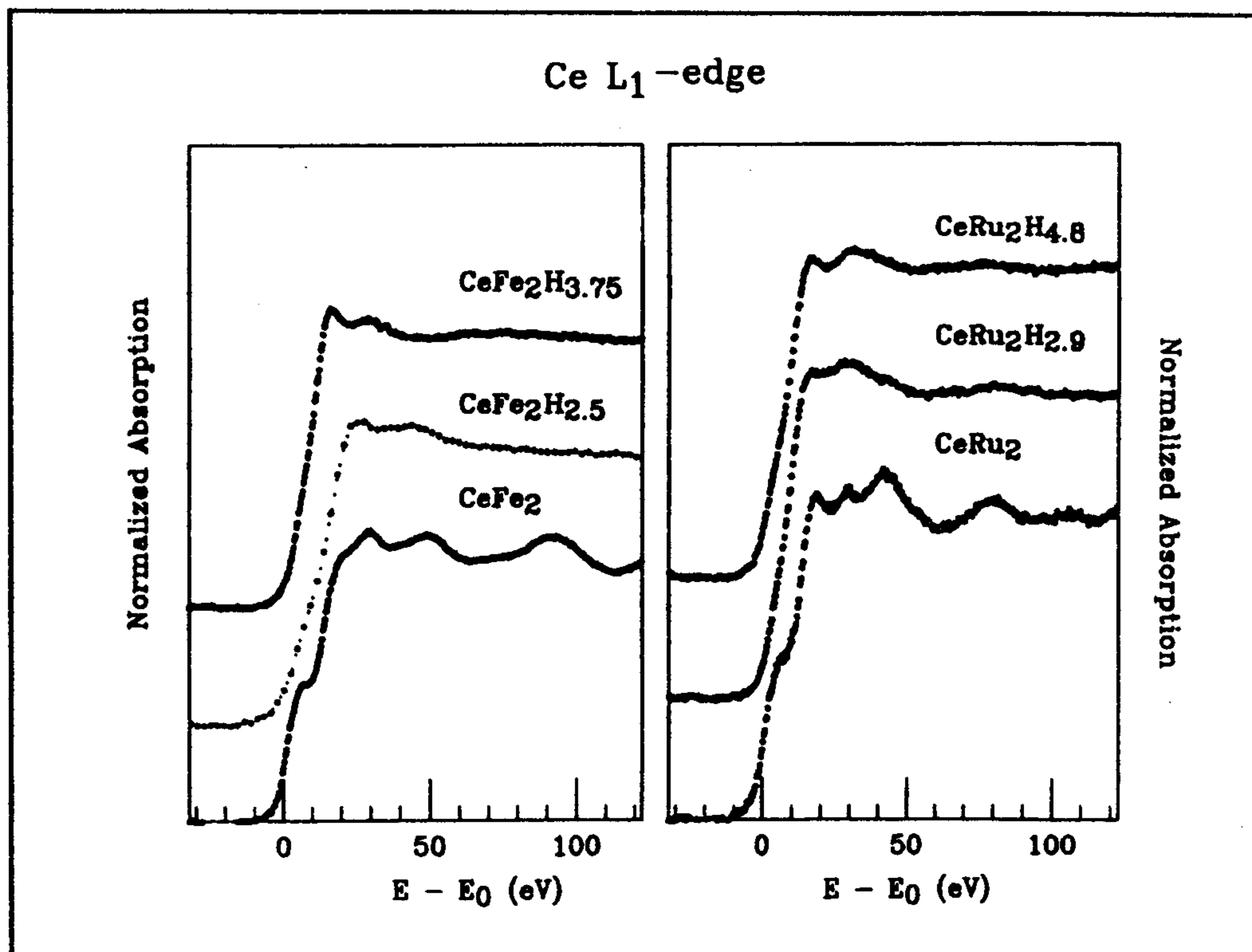
Ce L₁−edge

Figure 9 – Comparison between the experimental XANES spectra at the cerium L_1-edge in the case of the CeFe₂H$_x$ (left panel) and CeRu₂H$_x$ (right panel) compounds.
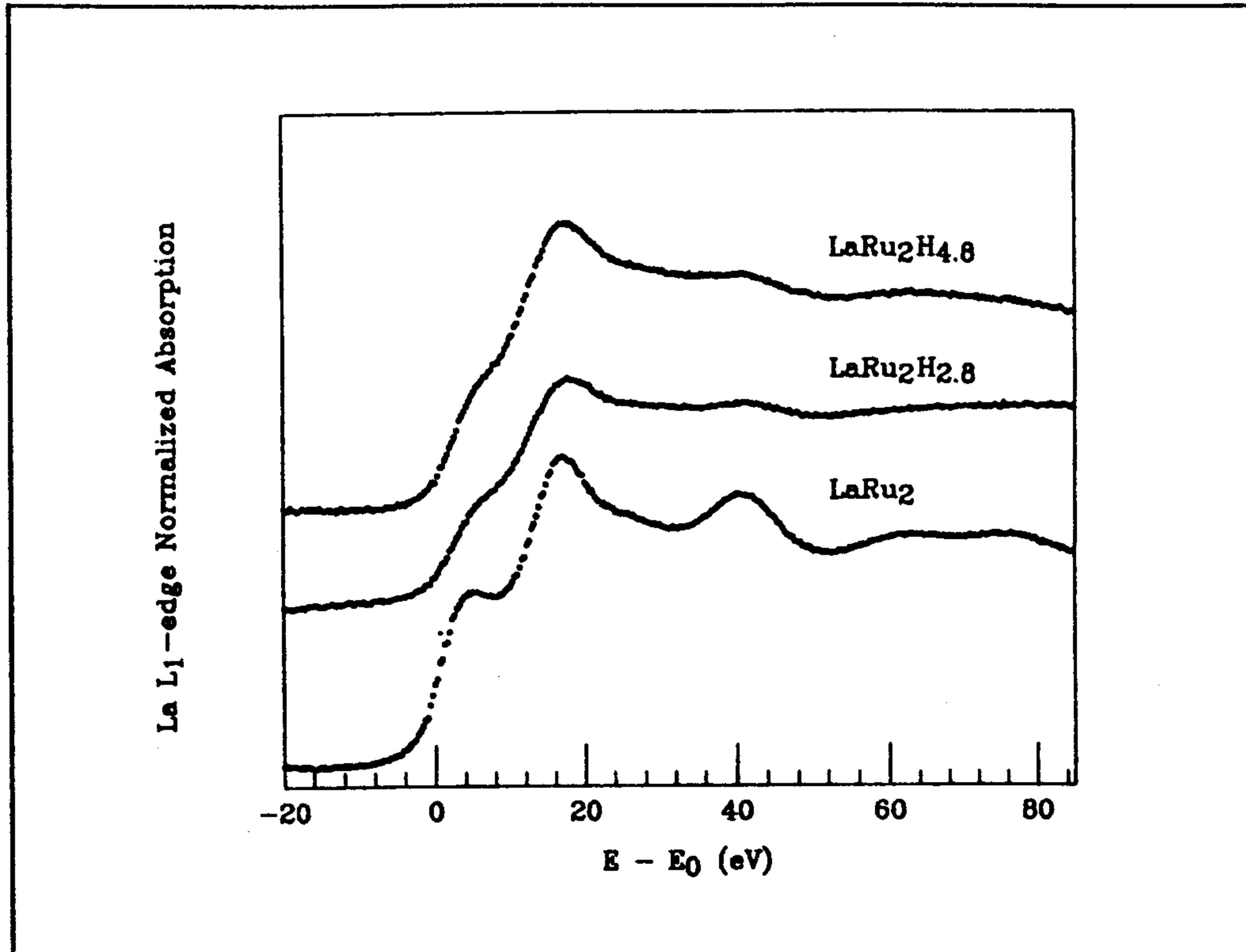
Figure 10 – Comparison between the experimental XANES spectra at the La L_1-edge in the case of the $LaRu_2H_\chi$ compounds.